Sensitivity of land use change emission estimates to historical land use and land cover mapping

Shushi Peng, Philippe Ciais, Fabienne Maignan, Wei Li, Jinfeng Chang, Tao Wang, Chao Yue

AGU PUBLICATIONS

Global Biogeochemical Cycles

RESEARCH ARTICLE
10.1002/2015GB005360

Special Section:
Global Land-Use Change and Carbon/Climate Dynamics

Sensitivity of land use change emission estimates to historical land use and land cover mapping

Shushi Peng[1], Philippe Ciais[1,2], Fabienne Maignan[2], Wei Li[2], Jinfeng Chang[2], Tao Wang[3,4], and Chao Yue[2]

[1]Sino-French Institute for Earth System Science, College of Urban and Environmental Sciences, Peking University, Beijing, China, [2]Laboratoire des Sciences du Climat et de l'Environnement, LSCE/IPSL, CEA-CNRS-UVSQ, Université Paris-Saclay, Gif-sur-Yvette, France, [3]Key Laboratory of Alpine Ecology and Biodiversity, Institute of Tibetan Plateau Research, Chinese Academy of Sciences, Beijing, China, [4]CAS Center for Excellence in Tibetan Plateau Earth Sciences, Chinese Academy of Sciences, Beijing, China

Key Points:
- Five transition rules with two reconstruction methods are used to reconstruct LULCC maps
- The total area of forest loss is highly correlated with the total simulated ELUC (R^2=0.83, P<0.001) across the reconstructed PFT maps
- Available forest area censuses can be used as a constraint to reconstruct historical LULCC maps

Supporting Information:
- Supporting Information S1

Correspondence to:
S. Peng,
speng@pku.edu.cn

Citation:
Peng, S., P. Ciais, F. Maignan, W. Li, J. Chang, T. Wang, and C. Yue (2017), Sensitivity of land use change emission estimates to historical land use and land cover mapping, *Global Biogeochem. Cycles*, *31*, 626–643, doi:10.1002/2015GB005360.

Received 16 DEC 2015
Accepted 8 MAR 2017
Accepted article online 10 MAR 2017
Published online 11 APR 2017

Abstract The carbon emissions from land use and land cover change (E_{LUC}) are an important anthropogenic component of the global carbon budget. Yet these emissions have a large uncertainty. Uncertainty in historical land use and land cover change (LULCC) maps and their implementation in global vegetation models is one of the key sources of the spread of E_{LUC} calculated by global vegetation models. In this study, we used the Organizing Carbon and Hydrology in Dynamic Ecosystems terrestrial biosphere model to investigate how the different transition rules to define the priority of conversion from natural vegetation to agricultural land affect the historical reconstruction of plant functional types (PFTs) and E_{LUC}. First, we reconstructed 10 sets of historical PFT maps using different transition rules and two methods. Then, we calculated E_{LUC} from these 10 different historical PFT maps and an additional published PFT reconstruction, using the difference between two sets of simulations (with and without LULCC). The total area of forest loss is highly correlated with the total simulated E_{LUC} ($R^2 = 0.83$, $P < 0.001$) across the reconstructed PFT maps, which indicates that the choice of transition rules is a critical (and often overlooked) decision affecting the simulated E_{LUC}. In addition to the choice of a transition rule, the initial land cover map and the reconstruction method for the reconstruction of historical PFT maps have an important impact on the resultant estimates of E_{LUC}.

1. Introduction

The net flux of CO_2 from land use and land cover change (LULCC) is an important component of the perturbation of the global carbon cycle caused by human activities [*Houghton et al.*, 2012; *Le Quéré et al.*, 2015]. Land use emissions (E_{LUC}) started well before the onset of the Industrial Era (1750) when emissions from fossil fuel burning began to rise [*Pongratz et al.*, 2009]. From 1870 to today, the cumulative carbon emissions from LULCC (145 ± 50 Pg C) amounts to about 33% of the total anthropogenic carbon emissions [*Le Quéré et al.*, 2015]; it is about 20% (73.5 ± 27.5 Pg C) of the emissions during the period 1959–2013 [*Le Quéré et al.*, 2015]. In global annual carbon budget assessments from the Global Carbon Project (GCP [*Le Quéré et al.*, 2015]), the net land carbon flux is estimated as the residual in the balance between fossil fuel and cement production emissions, and the atmospheric CO_2 growth and ocean carbon uptake. The net land carbon flux itself is the sum of E_{LUC} and a residual carbon sink over land to close the land C budget. With this method [*Le Quéré et al.*, 2015], any systematic error in the mean value of E_{LUC} translates into a bias of the same magnitude and opposite sign in the residual land carbon sink. Further, land use change emissions have a larger uncertainty than fossil fuel emissions, atmospheric growth rate, and ocean uptake [*Houghton et al.*, 2012; *Ciais et al.*, 2013; *Le Quéré et al.*, 2015; *Ballantyne et al.*, 2015], and this uncertainty dominates the uncertainty in the residual land sink.

Over the last three decades, E_{LUC} emissions decreased from 1.4 ± 0.5 Pg C yr^{-1} in the 1980s to 0.9 ± 0.5 Pg C yr^{-1} during the period 2004–2013, and the uncertainty of LULCC emissions is still large in the global carbon budget (± 0.5 Pg C yr^{-1}) [*Le Quéré et al.*, 2015]. To improve assessments of global and regional carbon budgets, the developers of global terrestrial biosphere models have been working to reduce the uncertainty of historical and current LULCC emissions [e.g., *Shevliakova et al.*, 2009; *Piao et al.*, 2009; *Reick et al.*, 2013; *Wilkenskjeld et al.*, 2014], but the spread of model results for E_{LUC} remains large [*Le Quéré et al.*, 2015].

The factors that induce large uncertainty in E_{LUC} estimates are summarized in the previous study [e.g., *Houghton et al*., 2012; *Pongratz et al*., 2014; *Goll et al*., 2015*; Stocker and Joos*, 2015]: (1) different definitions in different approaches have been applied to estimate historical E_{LUC} [*Pongratz et al*., 2014; *Gasser and Ciais*, 2013; *Stocker and Joos*, 2015], including coupled carbon-climate model simulations [e.g., *Pongratz et al*., 2009; *Stocker et al*., 2014], off-line (uncoupled) dynamic global vegetation model (DGVM) simulations [e.g., *McGuire et al*., 2001; *Piao et al*., 2009; *Jain et al*., 2013; *Le Quéré et al*., 2015], and bookkeeping models [*Houghton*, 2003; *Hansis et al*., 2015]; (2) uncertainty in historical cropland and pasture area [*Houghton et al*., 2012]; (3) uncertainty in historical land cover transitions upon changes in cropland and pasture area; (4) uncertainty in natural and agricultural ecosystems carbon density [*Hansis et al*., 2015]; and (5) uncertainty in ecosystem responses to external drivers (e.g., climate change, ambient CO_2, and nitrogen deposition) and LULCC processes. In the previous E_{LUC} estimates, Food and Agriculture Organization (FAO) forestry data were used in bookkeeping method [*Houghton*, 2003], and History Database of the Global Environment (HYDE) data incorporating FAO agricultural data were used to infer the land cover transitions in DGVMs. Compared with the decrease in global forest area by $\sim 8 \times 10^6$ km^2 from 1901 to 2005 in *Houghton* [2008], the DGVMs in the project "Trends and drivers of the regional-scale sources and sinks of carbon dioxide" (TRENDY) nine-model comparison project, the estimated decrease in global forest area from 1901 to 2005 ranged from 2.2×10^6 km^2 by Vegetation Integrative SImulator for Trace gases (VISIT) to 16.9×10^6 km^2 by Organizing Carbon and Hydrology in Dynamic Ecosystems (ORCHIDEE), even though the same HYDE cropland and pasture historical land use data were used in all the models. How to fill the "gap" between forestry data used in bookkeeping method and agricultural data used in DGVMs (related to the uncertainty of number 3 mentioned above) is the first goal of this study.

To assess the biogeophysical and biogeochemical impacts of LULCC at global and regional scales, annual spatially and temporally explicit data sets of LULCC data are needed for process-based terrestrial biosphere models [e.g., *Piao et al*., 2009; *Jain et al*., 2013; *Le Quéré et al*., 2015; *Devaraju et al*., 2015]. Historical spatially gridded data sets of cropland and pasture have been reconstructed from land use statistics and population growth [e.g., *Ramankutty and Foley*, 1999; *Klein Goldewijk*, 2001; *Hurtt et al*., 2006, 2011; *Pongratz et al*., 2008; *Klein Goldewijk et al*., 2011]. When incorporating these gridded cropland and pasture data sets into annual land use/cover change maps for use in process-based terrestrial biosphere models, rules and assumptions are needed about how to allocate new cropland and pastures from the previous areas of forest, shrub, or natural grassland [e.g., *Shevliakova et al*., 2009; *Meiyappan and Jain*, 2012; *Jain et al*., 2013; *Brovkin et al*., 2013; *Reick et al*., 2013; *Hansis et al*., 2015].

Several allocation rules have been proposed in previous studies. Generally, there are three published rules for expansion or abandonment of agricultural land: (1) proportional reduction or expansion of existing natural PFTs within the grid for both cropland and pasture [*Meiyappan and Jain*, 2012; *Jain et al*., 2013]; (2) preferential reduction or expansion of natural grassland for pasture and proportional reduction or expansion of existing natural PFTs within the grid for cropland [*Houghton et al*., 1983*; Reick et al*., 2013]; and (3) preferential reduction or expansion of natural grassland for both cropland and pasture (The Hadley Centre Global Environmental Model (HadGEM) model in *Brovkin et al*. [2013]). Besides the above rules, for the abandonment of agricultural lands, there is one variant of rule 1: the dominant potential vegetation type was taken for abandonment of agricultural land [*Jain et al*., 2013]. For the terrestrial biosphere model activated with dynamic vegetation, the reduction or expansion of natural PFTs for agricultural land is simulated by dynamic vegetation module, but accurate rules for past land cover transitions is a limiting factor to determine how agricultural area should be allocated in grid cells where natural vegetation can also change [*Strassmann et al*., 2008]. Besides these rules, *Pongratz et al*. [2008] used annual 5 min spatial resolution cropland maps and the potential vegetation map of [*Ramankutty and Foley*, 1999] to define the source vegetation type for allocation of cropland in each 0.5° grid cell and used a rule of preferential allocation of pasture on natural grassland. In multimodel comparison projects [e.g., *Le Quéré et al*., 2015], land use modelers easily agree to adopt the same *agricultural* cover history, i.e., time varying maps of cropland and pasture, but still generate different *land cover* histories, because of (1) different rules for deciding which type of vegetation is replaced by agriculture, (2) different natural vegetation types prescribed or derived from dynamic vegetation module, and (3) different processes for LULCC such as wood harvest, shifting cultivation, net transitions, and gross transitions in different models. Table S1 in the supporting information summarizes these differences in the TRENDY models [*Best et al*., 2011; *Clark et al*., 2011; *Ito and Inatomi*, 2012; *Kato et al*., 2013; *Krinner et al*., 2005; *Oleson*

et al., 2013; *Reick et al*., 2013; *Sitch et al*., 2003; *Smith et al*., 2001; *Stocker et al*., 2014; *Zaehle and Friend*, 2010]. Five out of the nine TRENDY models used prescribed LULCC maps as input, and at least six out of the nine models used prescribed allocation rules for agricultural expansion and reduction (Table S1). Different rules for agricultural expansion are thus one of the reasons for the large spread of E_{LUC} estimates from process-based models [e.g., *Houghton et al*., 2012; *Le Quéré et al*., 2015]. The land use transition rules are not sufficiently constrained due to missing information, and assessing the impact of the choice of different rules on simulated LULCC emission histories is the main goal of this study.

In this paper, we investigate how historical E_{LUC} changes when different rules are used to define the land cover transitions between natural vegetation and agriculture in the same terrestrial biosphere model. To do so, we combine the Land Use Harmonization historical (LUH-HYDE3.1) [*Hurtt et al*., 2011] data for the period 1500–2005 with current and past land cover maps to reconstruct 10 different sets of historical maps for the 13 PFTs of the ORCHIDEE terrestrial biosphere model (see Table S2) applying five different rules with both backward and forward methods. Then we use the ORCHIDEE model to quantify the sensitivities of the estimated LULCC emissions to different sets of historical plant functional type (PFT) maps. ORCHIDEE is one of the typical terrestrial biosphere model for estimates of LULCC emissions (Table S1). Note that ORCHIDEE r2061 applied to estimate LULCC emissions in this study does not include shifting cultivation and wood harvest processes, which can cause bias of LULCC emissions presented here. Note that most of TRENDY models do not have wood harvest and shifting cultivation either (except for Jena Scheme for Biosphere–Atmosphere Coupling in Hamburg (JSBACH) and VISIT, Table S1). The details of the reconstruction of land cover change maps and PFT historical maps from the harmonized land use data [*Hurtt et al*., 2011] are presented in section 2 for different rules. The changes in global and regional forest area from different sets of historical PFT maps are shown in section 3. The sensitivities of LULCC emissions to different LULCC maps are presented in section 4. Conclusions are summarized in section 5.

2. Data Sets and Methods

2.1. Historical Cropland and Pasture Data

We used the LUH-HYDE3.1 historical harmonized global gridded land use data set produced by *Hurtt et al.* [2011, luh.umd.edu]. In this data set, the time varying spatial distribution of cropland and pasture, ice/water, and urban land is from the HYDE 3.1 database [*Klein Goldewijk et al*., 2011]. These four land use types were provided every 10 years from 1500 to 2000 and in 2005 at a resolution of $5' \times 5'$ in the original HYDE3.1 data set and were aggregated into $0.5° \times 0.5°$ and linearly interpolated in time to produce annual gridded cropland, pasture, ice/water, and urban land fractions during the period 1500–2005 as part of the LUH-HYDE3.1 product. The LUH-HYDE3.1 product is used to reconstruct historical land use change emissions with vegetation models in GCP and Coupled Model Intercomparison Project Phase 5 (CMIP5) projects [*Brovkin et al*., 2013; *Le Quéré et al*., 2015]. Modelers can choose to use the annual fractional data provided by LUH-HYDE3.1, but in that case, they need to define the rules that set which type of natural vegetation is destroyed/expanded when new cropland or new pasture is created/abandoned.

2.2. Historical Forest Area Data at Continental Scale

To our knowledge, there is no global gridded reconstruction of historical forest area for the industrial era, which is the reason why modelers have to assume rules to define the natural PFT which gets destroyed when agriculture appears in a grid cell. Yet there is a global reconstruction of annual forest area at the scale of nine large regions of the globe, from 1850 to 1990; this was assembled by *Houghton* [2003, 2008] and is based on national forest area statistics. Figure S1 maps these nine regions.

2.3. Initialization of the Backward PFT Reconstruction Method

The so-called "backward method" of reconstructing PFT maps starts from an observed PFT distribution during the current period. It then follows time backwards applying at each time step the agricultural area changes between two consecutive years from LUH-HYDE3.1 together with the rules defining which type of natural vegetation is impacted by agricultural area change. In this method, the result is a set of annual PFT maps up until the assumed starting year of land use change (1500). In reconstructing historical PFT maps using the backward method, we started with the European Space Agency (ESA) Climate Change Initiative (CCI) land cover map for the 5 year period from 2003 to 2007 [*European Space Agency (ESA)*, 2014]. The ESA CCI land

cover map is derived from Medium-Resolution Imaging Spectrometer (MERIS) and SPOT vegetation satellite data, with a spatial resolution of 300 m [*ESA*, 2014]. The 22 original land cover classes from the ESA CCI map were aggregated into the 13 PFTs of ORCHIDEE [*Krinner et al*., 2005] using the method of *Poulter et al.* [2015], which combined a cross-walking table between satellite land cover classes and PFTs of ORCHIDEE with the Köppen-Geiger climate classification. The resulting spatial distribution of forest, natural grassland, cropland, and pasture is shown in Figure S3. The areas of crops and pasture from the ESA CCI map are not spatially consistent with that from LUH-HYDE3.1 data, which are from HYDE3.1 (Figure S3 and S4). The total crop area in ESA CCI is 18.8×10^6 km^2 (15.6×10^6 km^2 in HYDE3.1), and the total grassland area is 25.0×10^6 km^2. It is not easy to distinguish cropland and pasture from grassland by remote sensing and the classification of pasture and cropland may thus be uncertain in ESA CCI. Thus, we adjusted the ESA-CCI map by reducing the fractions of cropland in each 0.5° grid cell if they exceeded the values of LUH-HYDE3.1. In those grid cells where croplands had to be reduced, the area of grassland was increased to compensate. We used the total grassland area in ESA CCI (25.0×10^6 km^2) minus the pasture area from HYDE3.1 (33.4×10^6 km^2 in HYDE3.1) to separate pasture and natural grassland area in ESA CCI. In those grid cells where the grassland area in ESA CCI is smaller than pasture from HYDE3.1, the area of pasture was set as the total grassland area. After the adjustment, the total crop and pasture areas are 12.7×10^6 km^2 and 18.8×10^6 km^2, respectively. With this adjustment, the adjusted crop and pasture areas are smaller than in LUH-HYDE3.1, which has a crop area of 15.6×10^6 km^2 and a pasture area of 33.4×10^6 km^2 in 2005. The reason for this is inconsistencies between ESA CCI land cover map in 2005 and LUH-HYDE3.1, with some 0.5° grid cells having agriculture on one map and not in the other. Note that in addition to grasslands, pasture in LUH can include ecosystems with a significant fraction of bare soil like steppe, shrubs, and ecosystems with a significant tree fraction like savannas where animals graze, whereas here we only included grassland from ESA-CCI as pasture because the 13 PFTs of ORCHIDEE do not include shrubs and savannas PFTs. For a more consistent map between ESA CCI and LUH, the cross-walking table for ORCHIDEE 13 PFTs [*Poulter et al*., 2015] could be modified in future studies to allow pasture including some land cover classes which have a significant faction of bare soil or trees. The consequences of these inconsistencies are discussed in section 3. Hereafter, we use this merged ESA CCI-LUH map for the 2005 period to reconstruct PFT maps backwards in time until 1500.

2.4. Initialization of the Forward PFT Reconstruction Method

The "forward method" to reconstruct PFT maps requires an initial PFT map for the year 1500. Previous studies using the forward method generally start with a potential vegetation map before the industrial era [e.g., *Meiyappan and Jain*, 2012]. *Pongratz et al.* [2008] incorporated the Center for Sustainability and the Global Environment (SAGE) [*Ramankutty and Foley*, 1999] and HYDE [*Klein Goldewijk*, 2001] land use data to reconstruct a historical PFT maps from 800 to 1992 using a potential vegetation map for year 800 (hereafter, this data set is named as JP). The initial map of the year 1500 used for forward methods in this study is from *Pongratz et al.* [2008] for natural vegetation and LUH-HYDE3.1 for cropland and pasture. Figure S5 shows this map for forest, natural grassland, cropland, and pasture. The uncertainty of this initial map and its effects on the reconstructed maps are discussed in section 3.

2.5. Reconstructing PFT Maps

To comprehensively investigate effects of transition rules on reconstructed PFT maps, we considered two extreme rules (Rules 1 and 2) and three intermediate rules (Rules 3–5) as shown in Table 1. Rules used in previous publications are Rule 1 in the HadGEM model for CMIP5 [*Brovkin et al*., 2013], Rule 4 in *Houghton et al.* [1983] and *Reick et al.* [2013], and Rule 5 in *Jain et al*., [2013]. To complement these rules used in previous work, we added one complementary extreme rule (Rule 2) similar as Rule 1, but with a preferential allocation of cropland and pasture on forest. Then, in order to perfectly match the historical changes of forest area with Houghton's data during 1850–1990 and JP data before 1850 (no available continental statistic forest data before 1850), we also propose and test a new rule (Rule 3) where changes in total forest area (continental scale) must follow the data from Houghton et al. during 1850 1990 and from the JP data set during 1500–1850. Overall, the rank of preference for using forest for expansion of agriculture is Rule 2 > Rule 5 > Rule 4 > Rule 1, and the rank of preference for using natural grassland is the reverse (Rule 2 < Rule 5 < Rule 4 < Rule 1). The establishment of urban and agricultural areas upon forest is constrained by independent forest area data in Rule 3. We used the backward and the forward methods, each with the five different rules, to reconstruct 10 sets of historical PFT maps from 1500 to 2005 (Table 1).

Table 1. Summary of the Set of 10 Reconstructed PFT Histories in This Study. The Third and Fourth Columns Are the Names of PFT Histories Derived From Each Rule by Backward (BM) and Forward (FM) Methods, Respectively

	Description of Rules	Backward Method	Forward Method
Rule 1	The expansion of urban, cropland, and pasture in each grid cell is taken first from natural grassland, and then from forest if no natural grassland is available. The abandoned urban, cropland, and pasture are preferentially allocated to natural grassland, then to forest if natural grassland reach the potential maximum fraction of natural grassland defined by the potential vegetation map shown in Figure S2.	BM1	FM1
Rule 2	The expansion of urban, cropland, and pasture in each grid cell is taken first from forest, and then from natural grassland if no forest land is available. The abandoned urban, cropland, and pasture are preferentially allocated to forest, then to natural grassland if forest reach the potential maximum fraction of forest shown in Figure S2.	BM2	FM2
Rule 3	Same as Rule 2 but the total annual net change in forest area for each region is constrained to be the same as Houghton's data from 1850 to 1990 (Figure S1). For each region, if the total annual net deforestation/afforestation area from Rule 2 is different from changes in historical total continental forest area from Houghton's data during 1850–1990 and from JP data during 1500–1850, then a ratio of changes in total continental forest area Houghton's data or JP data to net deforestation/afforestation area from Rule 2 is applied to each grid in this region to adjust the annual changes in forest area to be the same as Houghton's data and JP data during the two periods, respectively, and the remaining agricultural land expansion/abandonment is first taken from/added to natural grassland then no agricultural land expansion if there is no more natural grassland.	BM3	FM3
Rule 4	Pasture is first taken from natural grassland, and then from forest if there is no available natural grassland. Expanded urban and cropland are taken in proportion from natural grassland and forest using the ratio of existing natural grassland to forest in the previous year by forward method and in the after year by backward method. The abandonment of pasture is preferentially allocated to natural grassland, and the abandonment of urban and cropland is proportionally given to natural grassland and forest.	BM4	FM4
Rule 5	The expansion of urban, cropland, and pasture in each grid cell is taken in proportion from natural grassland and forest using the ratio of existing natural grassland to forest in the previous year by forward method and in the after year by backward method. The abandonment of urban, cropland, and pasture is proportionally given to natural grassland and forest.	BM5	FM5

In the backward method (BM), we started from the merged ESA CCI land cover map in 2005 (see section 2.3), and applied annual changes of urban, cropland, and pasture between two consecutive years from LUH-HYDE3.1 following the rules in Table 1 to reconstruct the land cover map of the previous year, then recursively back to year 1500. We named the reconstructed land cover maps from Rule 1, Rule 2, Rule 3, Rule 4, and Rule 5 using the backward method BM1, BM2, BM3, BM4, and BM5, respectively (Table 1).

In the forward method (FM), we started from the initial map of 1500 (see section 2.4) and added the changes in urban, cropland, and pasture between two consecutive years from LUH-HYDE3.1 following the rules in Table 1, to reconstruct the land cover map of the next year, then iteratively up to the year of 2005. Similar to the backward method (BM), we named the five reconstructed land cover maps FM1–FM5 for each of the five rules. In both backward and forward methods, if forest and natural grassland are entirely depleted or reach the maximum allowed fraction, then cropland and pasture no longer expand or contract. Note that urban land expansion from forest or natural grassland is assumed to increase the area of bare ground since there is no urban land cover type in ORCHIDEE, and abandoned urban area is reverted back to forest or natural grassland depending on the rules in Table 1.

Table 1 summarizes the 10 PFT histories obtained with the two different methods and the five different rules. After deriving the land cover maps including bare ground, forest, natural grassland, and cropland, we converted them into 13 PFTs maps for ORCHIDEE (Table S2) as follows: in each grid for each year, the bare ground is PFT 1; the forest area is distributed into PFTs 2–9 by the fractions of PFTs 2–9 in the ESA CCI land cover map for the year 2005; grasslands (pasture + natural grassland) are distributed into PFTs 10 and 11 by the fractions of C3 versus C4 grass in ESA CCI land cover map; croplands are distributed into PFTs 12 and 13 by the fractions of C3 versus C4 crop in the ESA CCI land cover map. Besides the 10 sets of reconstructed PFT maps, the JP data were also translated to the PFTs of ORCHIDEE and used to define an additional PFT history (JP). Since no shrub PFT exists in ORCHIDEE, half of the shrub covered area in the JP data set was allocated to tree PFTs and the other half to grass PFTs. Note that the JP data set was produced with the forward method but with a variant of Rule 4, which thus does not correspond to any rule listed in Table 1.

In all these 11 reconstructed PFT maps, only net land use transitions are taken into account. For example, net increase in crop and pasture area between two consecutive years translates into the same area loss for forest

and natural grassland. This underestimates gross deforestation losses of carbon and carbon gains by secondary forest regrowth [e.g., *Shevliakova et al*., 2009; *Wilkenskjeld et al*., 2014].

2.6. LULCC Simulations

To evaluate and quantify land use change carbon emissions from historical land use and land cover change, we ran two sets of off-line simulations with ORCHIDEE (svn version r2061): one reference simulation forced by climate change, variable atmospheric CO_2, and LULCC (Sim 1; Table 2) and the other only with climate change and variable atmospheric CO_2 (Sim 2; Table 2). Atmospheric CO_2 concentration from 1500 to 1975 is from the Law Dome ice cores with a spline smoothing (75 year cutoff) (http://cdiac.ornl.gov/ftp/trends/co2/lawdome.smoothed.yr75), and a combination of ice core data and in situ atmospheric CO_2 measurements after 1975 (http://www.esrl.noaa.gov/gmd/ccgg/trends/global.html). The Climatic Research Unit-National Centers for Environmental Prediction 6 h climate forcing data from 1901 to 1990 was used in the simulations (http://dods.extra.cea.fr/data/p529viov/cruncep/readme.htm). For each reconstructed PFT history, we performed these two simulations (Sim 1 and Sim 2; see protocol in Table 2). E_{LUC}, defined as the difference in the net land atmosphere CO_2 exchange flux between Sim 1 and Sim 2 by off-line simulations, corresponds to the "D3 definition" of *Pongratz et al.* [2014], which is widely used in multimodel comparison projects such as TRENDY and Multi-Scale Synthesis and Terrestrial Model Intercomparison Project (MsTMIP) [*Piao et al*., 2009; *Sitch et al*., 2015; *Jain et al*., 2013; *Huntzinger et al*., 2013].

3. Global and Regional LULCC

3.1. Total Global LULCC Area

Since the forest area data used in BM3 and FM3 ends in 1990, the comparison of PFT maps between different rules and methods is only shown up to 1990. Table 3 shows the total global forest, natural grassland, cropland, and pasture area in 1500, 1850, and 1990, respectively. In the BM and FM PFT maps, the expansion of agriculture between 1500 and 1850 causes a loss of forest and natural grasslands in the range of 5.4 to 6.2×10^6 km^2. The expansion of urban area is almost negligible (0.03×10^6 km^2) from 1500 to 1850. Between 1500 and 1850, the total loss of forest ranges from 2.0×10^6 km^2 in BM5 to 5.2×10^6 km^2 in FM2, and the total loss of natural grasslands ranges from 0.8×10^6 km^2 in BM3 to 5.2×10^6 in BM5. For comparison, in the JP maps, the total forest and natural grassland areas decrease by 4.8×10^6 km^2 and 7.7×10^6 km^2, respectively.

The loss of natural vegetation (forest and grassland) from 1500 to 1850 is significant as it represents approximately 25% of the loss from 1850 to 1990 across the BM and FM maps; yet it is smaller than in the JP maps (41%). The expansion of cropland and pasture accelerated on the global scale, however, after 1850 (Figure S8). Because historical LULCC is much larger after 1850 than before, and because regional forest area data are only available from *Houghton* [2008] during the period 1850–1990, hereafter, we concentrate on LULCC results between 1850 and 1990 (Figure 1) and on the differences between the rules and the methods. Note that PFT maps in the year 1850 are different between the five rules in the FM method because of the accumulated effects of transition rules that occurred from 1500 to 1850 (Figure S6). These different maps in 1850 have effects on the allocations of the expansion of urban and agriculture on forest and natural grassland by FM. For the BM method on the other hand, the PFT maps in the year 1990 are similar between Rules 2 and 5, and slightly different with Rule 1.

Figure 1 shows the cumulative changes in forest, natural grassland, crop, and pasture areas from 1850 to 1990. During this period, the total loss of forest ranges from 1.6×10^6 km^2 in BM1 to 14.4×10^6 km^2 in BM2. Excluding the two extreme rules (Rule 1 and Rule 2) the total loss of forest ranges from 4.3×10^6 km^2 in BM4 to 10.2×10^6 km^2 in BM5. With the additional constraint added by the *Houghton* [2008] data, the loss of forest obtained in BM3 (FM3) (8.0×10^6 km^2) lies in between the two intermediate values given by BM4 (FM4) and BM5 (FM5) so does the loss of natural grassland. The five FM reconstructions have a smaller range of total forest loss than the BM maps (Figure 1). Reflecting preferences between rules for establishing agriculture on forest, the total loss of forest has the same rank between BM and FM: the largest forest loss being in BM2 (FM2), followed by BM5 (FM5), BM3 (FM3), BM4 (FM4), and BM1 (FM1). The loss of natural grasslands obtained with the five rules in BM and FM are ranked opposite (Figure 1). There is significantly negative correlation between the total forest loss and the loss of natural grasslands between 1850 and 1990 (Figure S7; $R = -0.98$, $P < 0.001$). Compared with BM3 and FM3, JP gives a slightly higher loss of forest (9.7×10^6 km^2) and a 3 times larger

Table 2. Simulation Protocol of Climate Change, CO_2, and Land Use and Land Cover Change for Sim 1 and Sim 2

Simulation	Spin-Up			Transient Run					
				1500–1900			1901–1990		
	CO_2	Climate	Land Cover	CO_2	Climate	Land Cover	CO_2	Climate	Land Cover
				Sim 1 Simulation					
S1-BM1	280 ppm	Cycled 1901–1920	BM1 1500	1500–1900	Cycled 1901–1920	BM1 1500–1900	1901–1990	1901–1990	BM1 1901–1990
S1-BM2	280 ppm	Cycled 1901–1920	BM2 1500	1500–1900	Cycled 1901–1920	BM2 1500–1900	1901–1990	1901–1990	BM2 1901–1990
S1-BM3	280 ppm	Cycled 1901–1920	BM3 1500	1500–1900	Cycled 1901–1920	BM3 1500–1900	1901–1990	1901–1990	BM3 1901–1990
S1-BM4	280 ppm	Cycled 1901–1920	BM4 1500	1500–1900	Cycled 1901–1920	BM4 1500–1900	1901–1990	1901–1990	BM4 1901–1990
S1-BM5	280 ppm	Cycled 1901–1920	BM5 1500	1500–1900	Cycled 1901–1920	BM5 1500–1900	1901–1990	1901–1990	BM5 1901–1990
S1-FM1	280 ppm	Cycled 1901–1920	FM1 1500	1500–1900	Cycled 1901–1920	FM1 1500–1900	1901–1990	1901–1990	FM1 1901–1990
S1-FM2	280 ppm	Cycled 1901–1920	FM2 1500	1500–1900	Cycled 1901–1920	FM2 1500–1900	1901–1990	1901–1990	FM2 1901–1990
S1-FM3	280 ppm	Cycled 1901–1920	FM3 1500	1500–1900	Cycled 1901–1920	FM3 1500–1900	1901–1990	1901–1990	FM3 1901–1990
S1-FM4	280 ppm	Cycled 1901–1920	FM4 1500	1500–1900	Cycled 1901–1920	FM4 1500–1900	1901–1990	1901–1990	FM4 1901–1990
S1-FM5	280 ppm	Cycled 1901–1920	FM5 1500	1500–1900	Cycled 1901–1920	FM5 1500–1900	1901–1990	1901–1990	FM5 1901–1990
S1-JP	280 ppm	Cycled 1901–1920	JP 1500	1500–1900	Cycled 1901–1920	JP 1500–1900	1901–1990	1901–1990	JP 1901–1990
				Sim 2 Simulation					
S2-BM1	280 ppm	Cycled 1901–1920	BM1 1500	1500–1900	Cycled 1901–1920	BM1 1500	1901–1990	1901–1990	BM1 1500
S2-BM2	280 ppm	Cycled 1901–1920	BM2 1500	1500–1900	Cycled 1901–1920	BM2 1500	1901–1990	1901–1990	BM2 1500
S2-BM3	280 ppm	Cycled 1901–1920	BM3 1500	1500–1900	Cycled 1901–1920	BM3 1500	1901–1990	1901–1990	BM3 1500
S2-BM3	280 ppm	Cycled 1901–1920	BM4 1500	1500–1900	Cycled 1901–1920	BM4 1500	1901–1990	1901–1990	BM4 1500
S2-BM3	280 ppm	Cycled 1901–1920	BM5 1500	1500–1900	Cycled 1901–1920	BM5 1500	1901–1990	1901–1990	BM5 1500
S2-FM1	280 ppm	Cycled 1901–1920	FM1 1500	1500–1900	Cycled 1901–1920	FM1 1500	1901–1990	1901–1990	FM1 1500
S2-FM2	280 ppm	Cycled 1901–1920	FM2 1500	1500–1900	Cycled 1901–1920	FM2 1500	1901–1990	1901–1990	FM2 1500
S2-FM3	280 ppm	Cycled 1901–1920	FM3 1500	1500–1900	Cycled 1901–1920	FM3 1500	1901–1990	1901–1990	FM3 1500
S2-FM4	280 ppm	Cycled 1901–1920	FM4 1500	1500–1900	Cycled 1901–1920	FM4 1500	1901–1990	1901–1990	FM4 1500
S2-FM5	280 ppm	Cycled 1901–1920	FM5 1500	1500–1900	Cycled 1901–1920	FM5 1500	1901–1990	1901–1990	FM5 1500
S2-JP	280 ppm	Cycled 1901–1920	JP 1500	1500–1900	Cycled 1901–1920	JP 1500	1901–1990	1901–1990	JP 1500

loss of grasslands (20.6×10^6 km^2) from 1850 to 1990. Since the historical regional forest area used in bookkeeping model [*Houghton*, 2003, 2008] is used to constrain the forest area in BM3 (FM3), the changes in regional forest area are consistent between bookkeeping model (using forest area data) and terrestrial biosphere model (based on changes in agricultural area data). In TRENDY models, compared with 6.1×10^6 km^2 loss of forest area during 1901–1990 in BM3 (FM3), six out of the nine models have higher loss of forest area ($7.1–14.8 \times 10^6$ km^2), and the other three models have smaller loss of forest area ($2.8–4.1 \times 10^6$ km^2).

The expansion of urban land (0.3×10^6 km^2) is dwarfed by the expansion of cropland ($7.8–9.2 \times 10^6$ km^2) and pasture ($12.1–14.8 \times 10^6$ km^2) during the period 1850–1990 both in the BM and FM methods. The area of cropland increases by 7.8×10^6 km^2 and 9.2×10^6 km^2 in BM and FM, respectively, which is comparable with the LUH-HYDE3.1 data (9.3×10^6 km^2) and JP (10.3×10^6 km^2). The smaller increase of cropland area in BM is

Table 3. Total Global Forest, Natural Grassland, Crop, and Pasture in the Years of 1500, 1850, and 1990

	Forest (km^2)			Natural Grassland (km^2)			Cropland (km^2)			Pasture (km^2)		
	1500	1850	1990	1500	1850	1990	1500	1850	1990	1500	1850	1990
BM1	46.9	44.6	43.0	36.5	33.0	12.5	2.0	4.8	12.7	1.6	4.5	18.5
BM2	61.2	58.3	44.0	22.2	19.2	11.5	2.0	4.8	12.7	1.6	4.5	18.5
BM3	56.6	51.9	44.0	27.2	26.5	11.5	2.0	4.8	12.7	1.2	3.7	18.5
BM4	50.1	47.9	43.6	33.2	29.7	11.9	2.0	4.8	12.7	1.6	4.5	18.5
BM5	56.0	54.0	43.8	27.3	23.5	11.6	2.0	4.8	12.7	1.6	4.5	18.5
FM1	52.7	50.1	42.7	41.1	37.5	21.7	2.3	5.4	14.6	2.4	5.5	19.2
FM2	52.7	47.6	36.0	41.1	40.0	28.3	2.3	5.4	14.6	2.4	5.5	19.2
FM3	52.7	48.0	40.0	41.1	39.9	26.3	2.3	5.4	14.6	2.4	5.1	17.3
FM4	52.7	49.8	42.0	41.1	37.8	22.3	2.3	5.4	14.6	2.4	5.5	19.2
FM5	52.7	49.2	39.8	41.1	38.4	24.5	2.3	5.4	14.6	2.4	5.5	19.2
JP	52.6	47.8	38.1	40.7	33.0	12.5	2.7	8.2	18.6	2.6	9.6	29.5

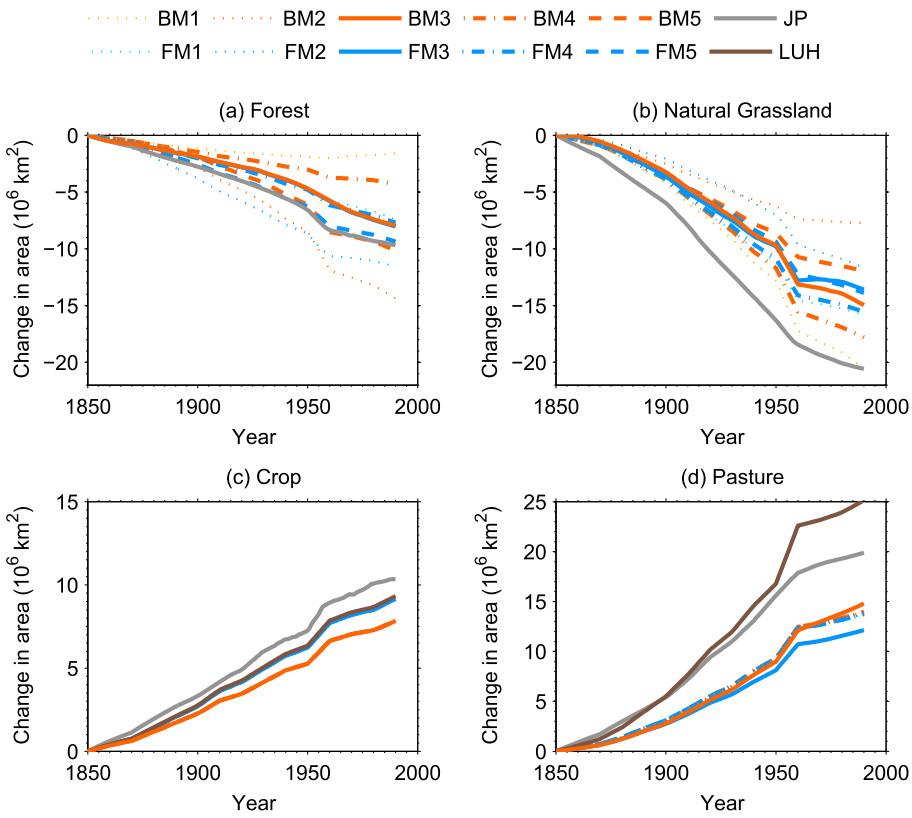

Figure 1. The total global changes in area of (a) forest, (b) natural grassland, (c) crop, and (d) pasture from 1850 to 1990.

because of the inconsistent cropland maps between LUH-HYDE3.1 and the ESA CCI land cover map in 2005 (Figure S3 and S4). The pasture area increases by 14.0–14.8 $\times 10^6$ km^2 and 12.1–13.7 $\times 10^6$ km^2 in BM and FM runs, respectively, which is lower than in LUH-HYDE3.1 (25.1 $\times 10^6$ km^2) and JP (19.9 $\times 10^6$ km^2). This smaller increase of pasture area in BM and FM compared to LUH-HYDE3.1 mainly results from the smaller pasture area in the initial map of 2005 in BM, and the fact that "pasture" in LUH-HYDE3.1 includes lands suitable for grazing in arid and hyperarid ecosystems with a large fraction of bare ground, as well as shrublands and some savannas, whereas only grasslands can be pasture in ORCHIDEE. For instance, LUH-HYDE3.1 pasture areas in central Australia, northwest China, North Africa and Middle East, and Siberia are higher than the total vegetated area in the BM and FM maps, which is set by land classified as bare ground in the ESA-CCI satellite land cover data (Figures S3 and S4). In all the rules (i.e., Rules 1–5), bare ground cannot be used for establishing agricultural land. Therefore, the increase of crop and pasture areas in BM and FM cannot match the pasture land of LUH-HYDE3.1.

Figure 2 shows the annual rates of change in forest, natural grassland, cropland, and pasture areas between 1850 and 1990. The annual increase rate of cropland and pasture slightly increased from 1850 to 1950 with a drop during the world wars and then presents an abrupt rise in the 1950s and returns back to loss rates similar to the 1940s thereafter. The forest area loss rate is close to zero in BM1 and BM4, and the largest in BM2, reaching up to -0.35×10^6 km^2 yr^{-1} in the 1950s. Between the five rules, differences in forest area loss rates can be explained by the underlying rules. Note that the increase of forest area loss in the 1950s in BM3 and FM3 is not so "abrupt" as the other rules, which use forest to take up the large increase of agricultural land at that time. Compared to BM3 and FM3, JP has a larger loss rate of forest before the 1970s, but smaller values after the 1970s. The loss rate of natural grasslands takes larger values than that of forest in all the maps, except in BM2. JP has a larger expansion rate of crops and a smaller expansion rate of pasture than LUH-HYDE3.1.

3.2. Regional LULCC Area

Figure 3 shows the spatial patterns of changes in forest and natural grassland areas from 1850 to 1990, negative values being a loss. Excluding the two extreme rules (Rule 1 and Rule 2), the forest area

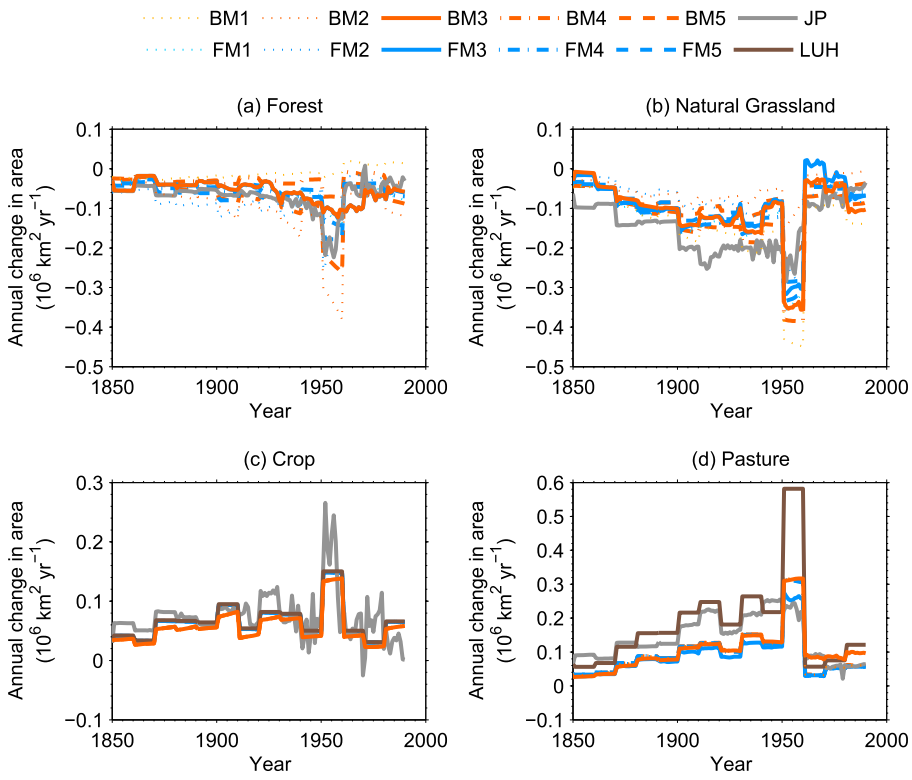

Figure 2. Annual total global changes in (a) forest, (b) natural grassland, (c) crop, and (d) pasture from 1850 to 1990.

decreased mainly in eastern North America, southeastern South America, tropical Africa, South and Southeast Asia, and China. Area of natural grasslands decreased in central North America, temperate South America, south of Africa, east of Europe, and Australia. The expansion of cropland and pasture has similar spatial patterns in LUH-HYDE3.1 and JP, but there are a few differences in some regions (Figure S9). The details of the distributions of crop and pasture have already been discussed by *Ramankutty and Foley* [1999], *Pongratz et al.* [2008], and *Hurtt et al.* [2011]. Here we focus on changes in the area of natural vegetation.

The regional changes in cumulative loss of forest and natural grassland areas are summarized in Figures 4 and 5. In BM3 and FM3, the forest loss is larger than the loss of natural grassland in South America and Southeast Asia, while in Eastern Europe, middle North America, Africa, and Australia, the loss of natural grassland is larger than that of forest. In North America, South and Central America, tropical Africa, China, and South and Southeast Asia, the total loss of forest area in BM3 being constrained by observations falls into the range between BM4 and BM5, which means that the expansions of crop and pasture were at the expense of both forest and natural grassland in these regions, and that rules with a preference for pasture expansion over natural grassland may underestimate deforestation (Figure 4). However, in BM3, the changes of forest area in the former Soviet Union and the Pacific Developed Regions are close to that in BM1 (assuming agricultural expansion comes at the expense of natural grassland), indicating that natural grassland is the main source for crop and pasture in these regions. In Europe, forest area increases after 1960 and is almost constant before 1960 in BM3, while reconstructed forest area decrease in BM4 and BM5 (Figure 4). The FM maps follow similar patterns than the BM maps, with closer values between FM3–FM5. BM3 and FM3 can also reproduce the net change of forest area independently assessed by *Fuchs et al.* [2014] in Europe, suggesting that the continental-scale data used by Houghton et al. are robust. During the period 1900–2010, 19.0% of the forest area in Europe was converted to other land use types, while 19.1% of other land use types was converted to forest according to *Fuchs et al.* [2014], leaving a net increase in forest area of 0.1%, which matches very well the forest area changes in BM3 and FM3 (0.1%). In North Africa and the Middle East, extreme assumption of agriculture expansion at the expense of forest (BM2) still leads to an underestimation of forest area loss. It is interesting to note that the forest area in China is modeled to increase from the 1970s to 1990 in BM3 and

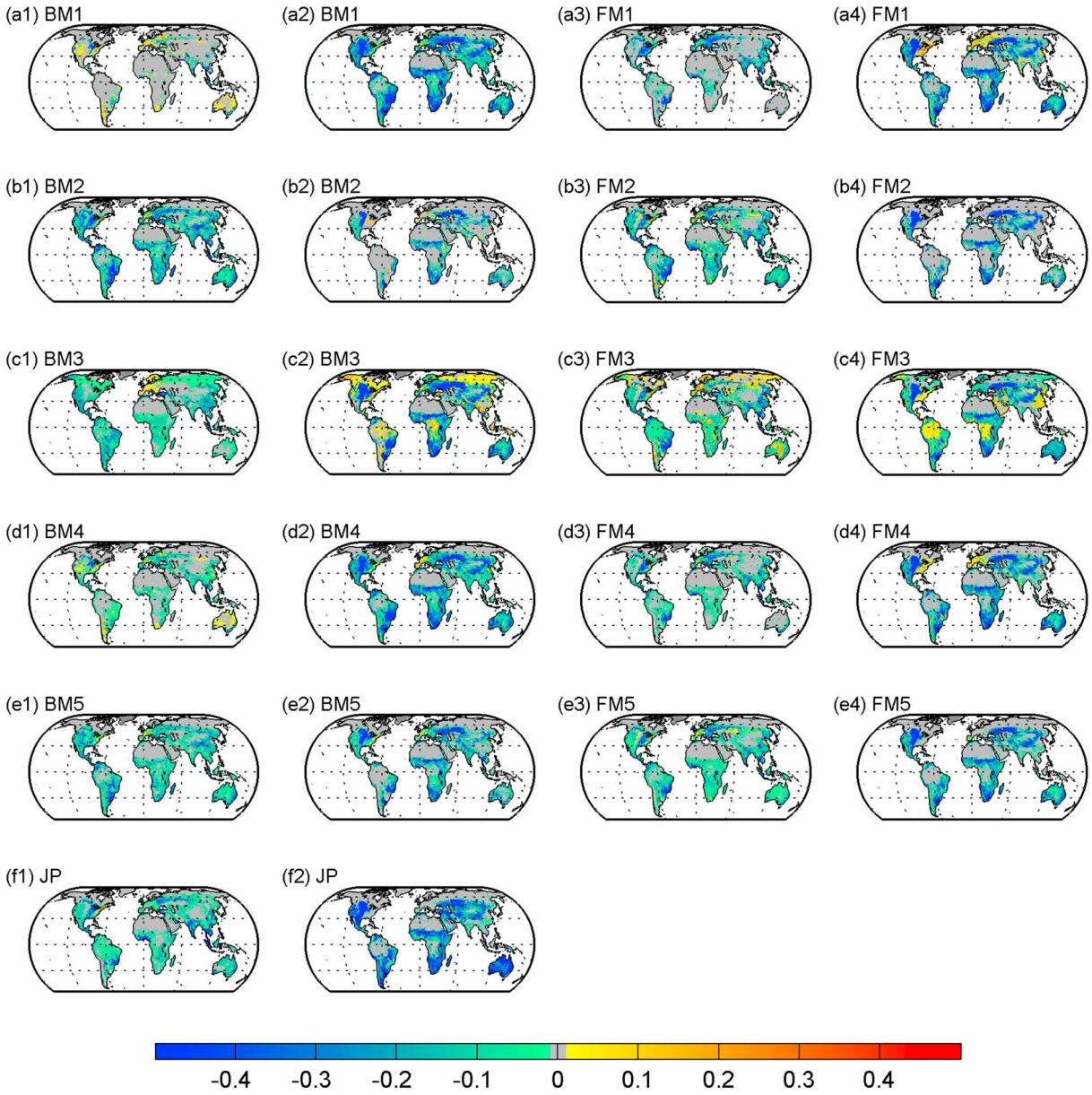

Figure 3. Spatial patterns of difference in forest ((first column) the BM and JP maps and (third column) the FM maps) and natural grassland ((second column) the BM and JP maps and (fourth column) the FM maps) area between 1850 and 1990. Units are percent of grid cell.

FM3, which is consistent with national forest census data [e.g., *He et al*., 2008], while forest area in China decreases in all the other methods (Figure 4).

The total loss of natural grassland area in BM3 falls into the range between BM4 and BM5 in most regions, except for Europe, North Africa and the Middle East, and the Former Soviet Union. In Europe, the higher loss of natural grasslands in BM3 (FM3) than BM1 (FM1) indicates that additional natural grasslands have been afforested besides the natural grasslands have been allocated to the expansion of cropland and pasture [*Fuchs et al*., 2014]. In the Former Soviet Union, the similar total loss of natural grasslands in BM3 than BM1 means that the establishment of cropland occurred mainly over natural grasslands in this region. Assuming that agricultural expansion comes at the expense of natural grassland (BM1), the loss of natural grasslands in North Africa and the Middle East is overestimated, which indicates agricultural land expansion here is at the expanse of forest area. However, the presence of shrublands and deserts in these regions may significantly impact our results because in our study, pasture can only be created from grasslands.

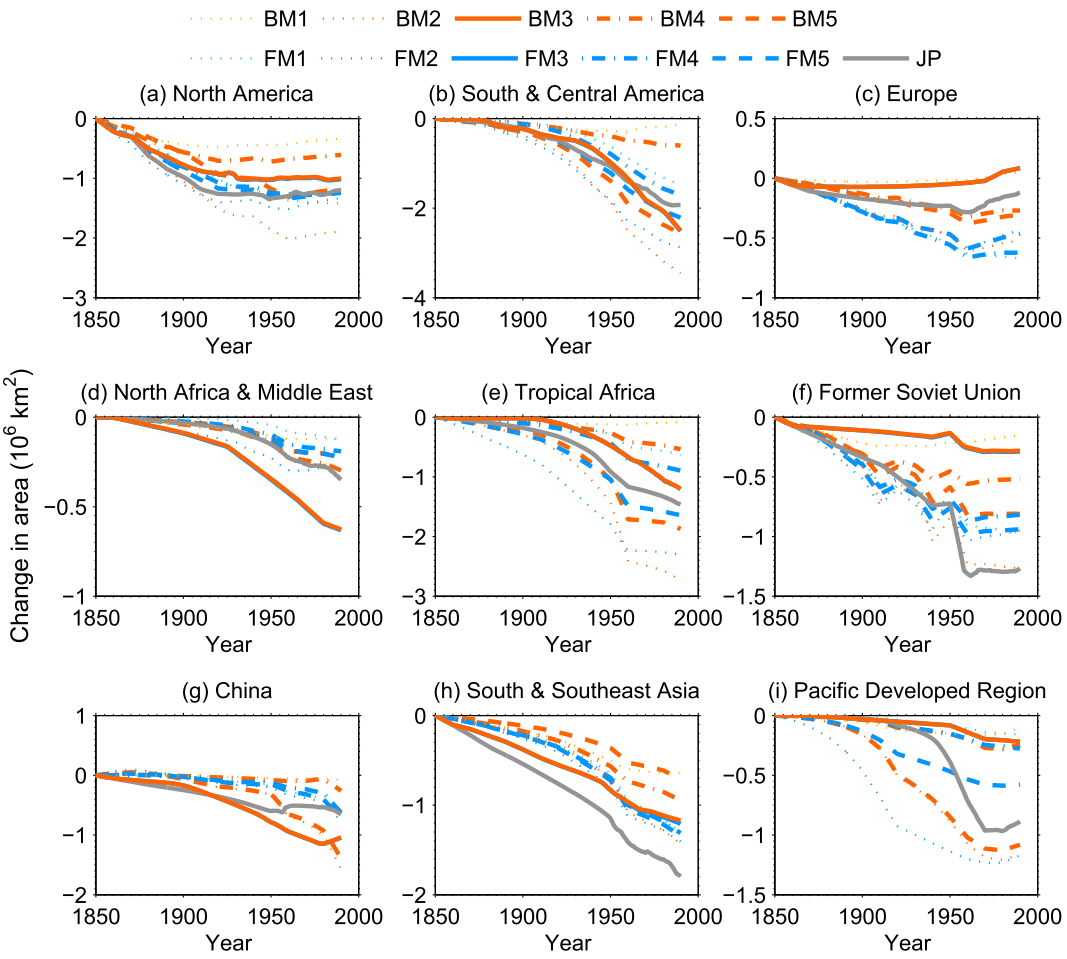

Figure 4. The total regional changes in area of forest from 1850 to 1990.

The allocations of regional expansion of agriculture on forest and natural grassland are different between the BM and FM maps (Figures 3–5 and Table S3). The global fractions of forest converted to cropland and pasture in JP (32%) are close to those of BM3 and FM3 (35% in BM3 and 37% in FM3). However, the regional fractions of forest converted to cropland and pasture are different between BM3 (FM3) and JP. Comparing BM3 and JP, the allocation of forest and natural grassland to agricultural land is significantly different in South and Central America, Europe, North Africa and the Middle East, the former Soviet Union, and China. In South and Central America, JP has more natural grassland (66%) than forest (34%) lost to agricultural land, while BM3 has more forest (56%) than natural grassland (44%) lost to agricultural land. In contrast, in the former Soviet Union, BM3 gives 90% of agricultural land expansion that is taken from natural grassland, compared with 62% only in JP. Overall, natural grassland is preferable for most agricultural land expansion in Europe, the former Soviet Union, and Pacific Developed Region, while both forest and natural grassland are used for agricultural land in other regions. With the same rule, BM and FM also have different results (Figures 1–5). Even in BM3 and FM3, the total loss of forest area is the same in these two maps, but the spatial patterns of changes in forest and natural grassland are different (Figure 3). For Rule 4, the total loss of forest area in FM4 is almost twice of that in BM4 at global and regional scales (Table S3). For Rule 5, the total loss of forest area in FM5 is slightly smaller than BM5 on global scale but with regional differences. For Rule 1 and Rule 2, the difference between FM and BM mainly results from the initial map in 1500 and in 2005, respectively, and from the maximum potential forest and grassland fractions used in BM. If different initial area of forest or natural grassland in a grid cell that experienced agricultural land expansion were applied with the same rule, the resulting decrease in forest and natural grassland can be different. The total forest area in the initial map of 1500 (52.7×10^6 km^2 with 6×10^6 km^2 shrublands as forest) derived from JP is used for FM. By comparison, a land cover map of 1765 (adjusted from *Ramankutty and Foley* [1999]) used as potential vegetation map by

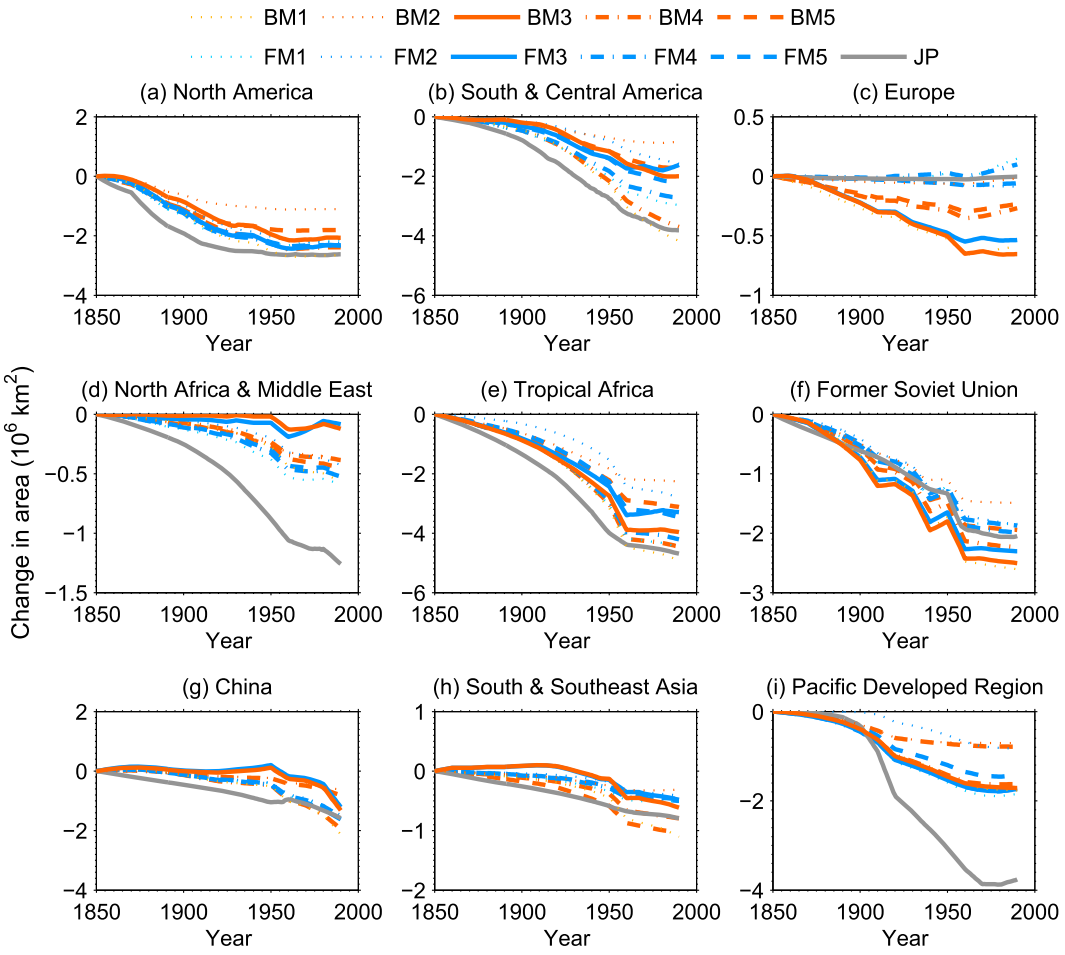

Figure 5. The total regional changes in area of natural grassland from 1850 to 1990.

Meiyappan and Jain [2012] provided 45.4×10^6 km^2 of total forest area, excluding shrublands. For Rule 4 and Rule 5, the proportion of forest and natural grassland in the initial map affects the allocation of agricultural land expansion in the FM and BM maps. Besides the effect of the initial map, the forward or backward directions in the reconstruction also affect the allocation of agricultural land expansion, since the proportions and locations of natural PFTs depend on the forward or backward directions. Therefore, the FM and BM, even with the same rule, have different results. A consistent potential vegetation map with satellite data could be useful for the FM method [*Meiyappan and Jain*, 2012]. In addition, as with arid regions of central Australia, the Middle East, northwestern China, and Mongolia (Figure S3 and S4), the area of vegetation used for pasture cannot be identified from satellite data (Moderate Resolution Imaging Spectroradiometer, ESA CCI in 2005). Satellites have limited ability to distinguish between pasture and natural grasslands or even between crops and pasture. We recommend the use of a more consistent initial map (total vegetated and forest area) with LUH-HYDE3.1 for future LULCC studies.

4. Sensitivity of LULCC Emission Estimates to Reconstruction of LULCC Maps

We now present the net land use change emissions E_{LUC} (Sim 1 and Sim-2) as calculated by ORCHIDEE for each of the10 PFT histories (Tables 2 and 4). Global cumulative E_{LUC} estimates during the periods 1500–1850 and 1850–1990 are presented in Table 4. Because Rule 1 and Rule 2 are extreme, we focused on more realistic cases of BM3–BM5, FM3–FM5, and JP. Between 1500 and 1850, with the BM and FM maps, the global cumulative E_{LUC} estimates range from 51 Pg C (BM4) to 78 Pg C (FM3), which is smaller than obtained with the JP maps (100 Pg C). The global cumulative E_{LUC} estimates in BM3 (FM3) is larger than that in BM4 (FM4) and BM5 (FM5), because BM3 and FM3 applied annual continental deforestation area from JP to constrain the change of forest area from 1500 to 1850, which is almost 2 times more deforestation than in

Table 4. Total Cumulative LULCC Emissions From All Global Land and the Nine Regions

	BM1	BM2	BM3	BM4	BM5	FM1	FM2	FM3	FM4	FM5	JP
Total Cumulative LULCC Emissions During 1500–1850 (Pg C)											
North America	3.6	7.2	7.1	4.7	4.6	10.8	11.9	13.7	11.2	11.3	16.2
South & Central America	10.7	15.3	11.1	10.6	14.1	9.1	10.4	9.4	8.7	9.7	13.6
Europe	6.1	7.9	16.5	6.0	6.1	10.5	11.0	16.1	11.0	10.6	20.1
North Africa and Middle East	0.1	0.2	0.1	0.1	0.1	0.1	0.2	0.2	0.1	0.1	0.2
Tropical Africa	5.6	7.4	6.4	5.7	6.6	5.9	6.3	5.2	5.9	6.1	5.4
Former Soviet Union	10.2	9.1	10.0	10.6	8.5	10.0	13.2	14.6	11.0	11.5	22.1
China	4.2	7.8	8.9	4.9	7.2	5.5	7.6	11.9	5.8	6.5	16.2
South and Southeast Asia	7.2	8.3	8.1	7.3	7.5	7.4	6.8	6.2	7.2	7.0	6.2
Pacific Developed Region	0.6	0.7	0.6	0.6	0.6	0.2	0.3	0.2	0.2	0.2	0.3
Global	48.2	63.9	68.8	50.6	55.3	59.4	67.7	77.6	61.1	63.1	100.3
Total Cumulative LULCC Emissions During 1850–1990 (Pg C)											
North America	14.1	30.8	16.5	17.5	18.2	32.2	30.3	26.3	31.0	29.8	32.3
South and Central America	12.6	41.0	24.2	16.0	31.9	22.6	34.3	32.9	24.2	28.2	17.5
Europe	5.7	12.1	6.1	7.8	8.3	13.7	13.2	7.9	14.1	13.3	8.8
North Africa and Middle East	0.7	1.2	1.5	1.0	1.0	0.8	1.3	1.8	1.0	1.1	1.0
Tropical Africa	7.2	17.3	11.9	8.6	12.6	9.0	16.9	11.6	10.2	12.8	8.4
Former Soviet Union	12.4	32.3	11.0	19.3	23.9	28.1	30.5	23.9	28.0	29.6	32.5
China	3.3	15.3	19.5	5.1	13.2	10.1	13.1	21.7	10.5	11.7	15.8
South and Southeast Asia	9.2	12.4	13.8	10.7	10.6	11.0	11.8	11.2	11.3	11.4	10.3
Pacific Developed Region	0.8	1.6	0.9	1.0	1.4	1.0	2.9	1.3	1.3	1.6	−1.6
Global	66.0	163.9	105.4	87.1	121.2	128.5	154.5	138.5	131.6	139.4	125.0

BM4–BM5 and FM4–FM5 (Table 3). The cumulative E_{LUC} from 1500 to 1850 is significant as it represents 31–39% of the cumulative E_{LUC} from 1500 to 1990 across the BM and FM maps, against 44% in the JP maps. Given that legacy emissions from previous land cover change are important [*Pongratz et al*., 2014; *Gasser and Ciais*, 2013], these substantial preindustrial LULCC emissions indicate that the carbon cycle is not in equilibrium in 1850, thus challenging the 1850 equilibrium assumption used in modeling studies such as TRENDY and MstMIP [see also *Pongratz et al*., 2009]. One difficulty for accurately accounting E_{LUC} in the preindustrial period by off-line modeling also arises from the lack of gridded climate forcing data. The cycled climate forcing during 1901–1920 used in the preindustrial period may thus cause biases in E_{LUC}.

Here we present the global and regional cumulative E_{LUC} during the period 1850–1990, especially for the 1980s. In ORCHIDEE, in the "realistic" cases BM3–BM5 and FM3–FM5, the global cumulative E_{LUC} estimates range from 87 Pg C (BM4) to 139 Pg C (FM5). This spread of global cumulative E_{LUC} results both from differences in forest area losses and in carbon density of biomes where deforestation happened. We found that the global cumulative E_{LUC} estimate from 1850 to 1990 is highly correlated with the total area of forest loss across the 10 reconstructed PFT maps and the JP maps as well (Figure 6; $R^2 = 0.83$, $P < 0.001$), which indicates the importance of transition rules on the estimation of E_{LUC}. Besides the total deforestation area, the location where forests are lost is also important for explaining E_{LUC} differences. For example, the total deforested area is the same in BM3 and FM3, but the global cumulative E_{LUC} estimates are 105 Pg C and 138 Pg C, respectively, because deforestation in FM3 happen in the area with higher biomass density (Figure 3).

According to ORCHIDEE results, during the period 1850–1990, the largest cumulative E_{LUC} is found in South and Central America (e.g., 24.2 Pg C in BM3 and 32.9 Pg C in FM3), followed by China (19.5 Pg C in BM3 and 21.7 Pg C in FM3) and North America (16.5 Pg C in BM3 and 26.3 Pg C in FM3) (Table 4). Compared with BM3 and FM3, JP has a larger cumulative E_{LUC} in North America (32.3 Pg C) and a smaller cumulative E_{LUC} in South and Central America (17.5 Pg C). More than 92% of total cumulative E_{LUC} are from six regions: South and Central America (23%), China (18%), North America (16%), South and Southeast Asia (13%), tropical Africa (11%), and the Former Soviet Union (10%) in BM3. The top six regions of total cumulative E_{LUC} in FM3 and JP are similar with the ones in BM3, but with more E_{LUC} from the Former Soviet Union (17% in FM3 and 26% in JP).

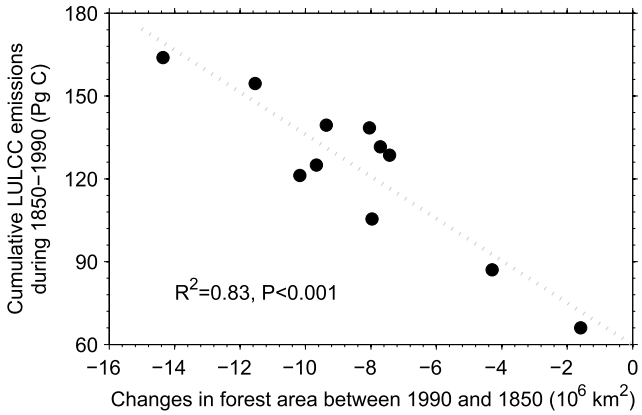

Figure 6. The relationship between cumulative global LULCC emissions during the period 1850–1990 and the changes in global forest area between 1990 and 1850 across different reconstruction LULCC maps.

Figure 7 shows the annual E_{LUC} from all historical PFT maps from 1850 to 1990. In BM3–BM5, FM3–FM5 and JP maps, before the 1940s, E_{LUC} keeps stable with interannual variations, then increases in the 1950s. After the 1950s, E_{LUC} decreases in the 1960s and then keeps stable after the 1970s. All historical PFT maps have similar decadal variations of E_{LUC} but different magnitudes. E_{LUC} in BM3 is smaller than in FM3 in all the decades, except the 1970s. E_{LUC} in JP is similar with FM3 and higher than BM3 before the 1950s, but lower than FM3 and BM3 after the 1950s.

The average E_{LUC} in BM3, FM3, and JP during the 1980s is of 1.1 Pg C yr^{-1}, 1.3 Pg C yr^{-1}, and 0.9 Pg C yr^{-1}, respectively, compared to the average of 13 estimates 1.1 ± 0.2 Pg C yr^{-1} summarized by *Houghton et al.* [2012]. E_{LUC} in BM4 is 0.7 Pg C yr^{-1} in the 1980s, lower than BM5 (1.2 Pg C yr^{-1}), while FM4 and FM5 have the same values (1.2 Pg C yr^{-1}). Our estimates of E_{LUC} in the BM3–BM5 and FM3–FM5 maps fall in the range of reported E_{LUC} in the 1980s [e.g., *Houghton et al.*, 2012].

The changes in annual E_{LUC} by region are shown in Figure 8. Small E_{LUC} are found in three regions (North Africa and the Middle East, Europe, and the Pacific Developed Region). Decreasing E_{LUC} is found in North America and Europe. Increased E_{LUC} are found in South and Central America, tropical Africa, China, and South and Southeast Asia, especially after the 1930s. Rather stable E_{LUC} is found for the Former Soviet Union, except for a peak in the 1950s and 1960s. There are larger differences in LULCC emissions between rules and methods in South and Central America after the 1910s and in China after the 1950s, and the former Soviet Union before the 1970s (Figure 8).

In China, national forest inventory data shows that forest area has increased since the 1980s [e.g., *Peng et al.*, 2014]. *Houghton* [2008] also show decreased E_{LUC} emissions because of afforestation/reforestation since the 1980s. With annual forest area constrained until 1990 at the scale of the East Asian region, as shown in

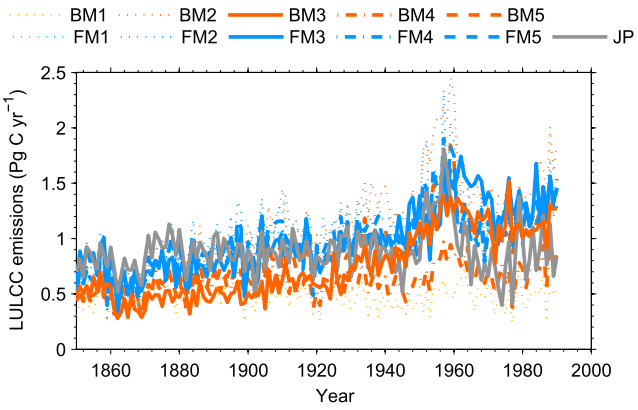

Figure 7. The annual global LULCC emissions from 1850 to 1990 for different reconstruction maps.

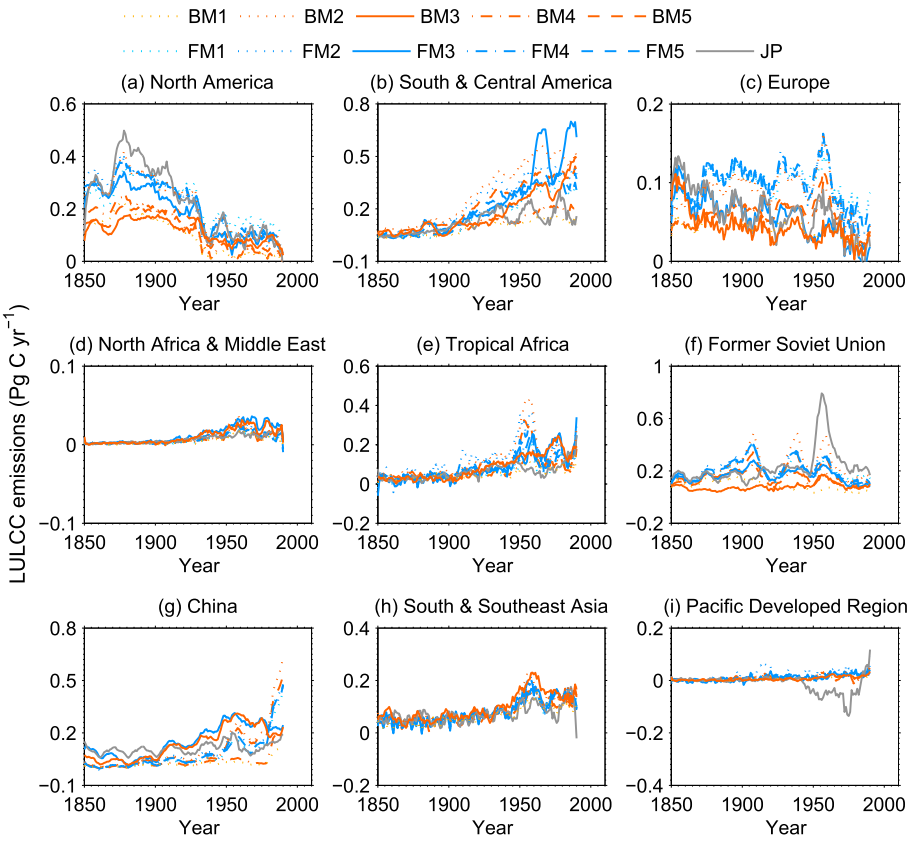

Figure 8. The regional LULCC emissions from 1850 to 1990 for different reconstruction maps.

Figure 4, BM3 and FM3 show an increased forest area in the 1980s, in contrast to decreased forest area in other reconstructed PFT maps. E_{LUC} in BM3 and FM3 decreased in China from the late 1970s, because of increasing forest area. This result contrasts with E_{LUC} simulated by terrestrial biosphere models for the past few decades, which is generally positive and increasing in China because of an unrealistic decrease in forest area in the LULCC input maps (e.g., TRENDY). BM3 and FM3 thus appear to be more realistic PFT reconstructions for China, consistent with regional data sets [*He et al.*, 2008].

In South and Central America, E_{LUC} in FM3 (0.64 Pg C yr^{-1}) is 4 times larger than in JP (0.16 Pg C yr^{-1}). About 50% of this range results from different deforested area, the other 50% being attributed to different locations of deforestation. However, in the bookkeeping method, the total deforestation area could be the main reason for the uncertainty if regional PFT shares the same ecosystem carbon density in that region. Besides uncertainty in carbon density of forests affected by LULCC, if better historical regional forest area census could be combined with satellite observations [e.g., *Imbach et al.*, 2015; *Hansen et al.*, 2013; *Kim et al.*, 2015], the BM3 or FM3 methods could be used to further reduce the uncertainty on E_{LUC} in that region.

Although a single model (ORCHIDEE) with prescribed LULCC maps and no dynamic vegetation was used to derive the sensitivity of E_{LUC} to LULCC maps and to the choice of agricultural land area allocation rules, the information about regional differences in allocation rules found in this study (preference of forest or grassland) should also be helpful for models activating dynamic vegetation module which do not need prescribed vegetation maps but do require allocation rules. In addition, our results imply that changes in planted forest area such as in China must be either prescribed over agricultural area in models with dynamic vegetation module or constrained using historical forest area in models with vegetation maps as input, to produce more realistic E_{LUC} estimates in global terrestrial biosphere models.

Considering uncertainty in the initial PFT map in the forward method, the backward method with a current map derived from satellite observations as initial map could be a better choice, provided that satellite land cover data can be reconciled with land use information. Alternatively, combining information from satellite

maps about natural vegetation boundaries into the potential preindustrial vegetation map may be another reasonable choice for the forward method [*Meiyappan and Jain*, 2012]. Yet natural vegetation shifts since preindustrial times (e.g., effects of CO_2 and climate and changes in fire regimes) may add uncertainty to this approach.

In addition, the spread of the loss of forest area closely relates to the initial forest cover map, which has been identified as a key source of uncertainty in E_{LUC} [*Goll et al*., 2015]. The key variable controlling E_{LUC}, the total area of forest loss, is determined by the initial forest cover map, transition rules, and the method of reconstruction as discussed above. Thus, the combination of a consistent initial forest cover map, application of the same transition rules, and national/regional forest area constraints is needed in future E_{LUC} estimation or multimodel comparison projects. Alternatively, the full coupled land use and land change model with integrated assessment model and Earth system model can be an integrated method to investigate and project E_{LUC} [*Di Vittorio et al*., 2014].

Besides the initial land cover map, transition rules and E_{LUC} estimation methods, land use forcing data (changes in agricultural land area) also contribute to uncertainty in E_{LUC} [e.g., *Jain and Yang*, 2005; *Shevliakova et al*., 2009]. *Shevliakova et al.* [2009], using a process-based terrestrial biosphere model and two land use data sets (HYDE and SAGE), found that the two land use data sets gave a 15% difference in estimated E_{LUC} over the period 1850–1990. There is a jump during the 1950s–1960s in LUH-HYDE3.1 data, cascading into E_{LUC} (Figure 7). This jump could be related to the jump in pasture areas (Figure 2), which results from inconsistency between FAO reports after 1961 and reconstructed pasture areas based on historical population densities before 1961. In addition, LULCC processes such as wood harvest, shifting cultivation, and other gross LULCC transitions at the spatial resolution where the model is applied are not included in the version of ORCHIDEE used in this study, which could cause further bias in E_{LUC} presented here [*Arneth et al*., 2017]. Caution is needed when comparing E_{LUC} in this study with estimates from models with wood harvest, shifting cultivation, and gross LULCC transitions.

5. Conclusions

In this study, we have shown that different transition rules for reconstructing historical PFT maps in a global terrestrial biosphere model result in large differences in E_{LUC}. Besides the two extreme transition rules, we found that the range of total global loss of forest area during the period 1850–1990 is $4.3–10.2 \times 10^6$ km^2 in the two published rules (Rule 4 and Rule 5), compared with 8.0×10^6 km^2 in the rule constraint with continental forest area (Rule 3). This uncertainty of loss of forest area by different transition rules can explain most of the uncertainty of E_{LUC} estimates by ORCHIDEE simulations. The BM3 and FM3 can improve the changes in forest area in continental regions, such as South and Central America, the Former Soviet Union, and China. Thus, the observed changes in annual forest area used as a constraint for reconstructing historical LULCC maps could be helpful to reduce the uncertainty of E_{LUC} induced by the total loss of forest area. Besides the transition rules, forward or backward method also has important impact on reconstructing historical PFT maps as well as E_{LUC}. The BM3/FM3 method as a hybrid method in this study should be adopted with a better initial land cover map for E_{LUC} in future multimodel comparison projects such as TRENDY and CMIP6.

Acknowledgments

S.P. and P.C. acknowledge support from the European Research Council through synergy grant ERC-2013-SyG-610028 "IMBALANCE-P." W.L. and Y.C. acknowledge support from the European FP7 project "LUC4C." We thank Natasha McBean and the investigators of the ESA Climate Change Initiative Land Cover Project 2014 for providing the 2005 land cover map. We thank J. Pongratz for providing the JP reconstruction of vegetation from 800 to 1992. The global and regional forest and natural grassland area in 1500, 1850, and 1990 are included as tables in the text and supporting information files. All the annual reconstructed maps from 1500 to 1900 are freely obtained from SP (e-mail: speng@pku.edu.cn).

References

Arneth, A., et al. (2017), Historical carbon dioxide emissions caused by land-use changes are possibly larger than assumed, *Nat. Geosci.*, *10*(2), 79–84.

Ballantyne, A. P., et al. (2015), Audit of the global carbon budget: Estimate errors and their impact on uptake uncertainty, *Biogeosciences*, *12*(8), 2565–2584, doi:10.5194/bg-12-2565-2015.

Best, M. J., et al. (2011), The Joint UK Land Environment Simulator (JULES), model description—Part 1: Energy and water fluxes, *Geosci. Model Dev.*, *4*(3), 677–699, doi:10.5194/gmd-4-677-2011.

Brovkin, V., et al. (2013), Effect of anthropogenic land-use and land-cover changes on climate and land carbon storage in CMIP5 projections for the twenty-first century, *J. Clim.*, *26*(18), 6859–6881, doi:10.1175/JCLI-D-12-00623.1.

Ciais, P., et al. (2013), Carbon and other biogeochemical cycles, in *Climate Change 2013: The Physical Science Basis. Contribution of Working Group I to the Fifth Assessment Report of the Intergovernmental Panel on Climate Change*, edited by T. F. Stocker et al., Cambridge Univ. Press, Cambridge, U. K., and New York.

Clark, D. B., et al. (2011), The Joint UK Land Environment Simulator (JULES), model description—Part 2: Carbon fluxes and vegetation dynamics, *Geosci. Model Dev.*, *4*(3), 701–722, doi:10.5194/gmd-4-701-2011.

Devaraju, N., G. Bala, and R. Nemani (2015), Modelling the influence of land-use changes on biophysical and biochemical interactions at regional and global scales, *Plant Cell Environ.*, *38*, 1931–1946, doi:10.1111/pce.12488.

Di Vittorio, A. V., et al. (2014), From land use to land cover: Restoring the afforestation signal in a coupled integrated assessment-earth system model and the implications for CMIP5 RCP simulations, *Biogeosciences*, *11*, 6435–6450.
European Space Agency (ESA) (2014), Land Cover CCI Product User Guide version 2.4, ESA 391 LC CCI project.
Fuchs, R., M. Herold, P. H. Verburg, J. G. P. W. Clevers, and J. Eberle (2014), Gross changes in reconstructions of historic land cover/use for Europe between 1900 and 2010, *Global Change Biol.*, *21*(1), 299–313, doi:10.1111/gcb.12714.
Gasser, T., and P. Ciais (2013), A theoretical framework for the net land-to-atmosphere CO_2 flux and its implications in the definition of "emissions from land-use change", *Earth Syst. Dyn.*, *4*(1), 171–186, doi:10.5194/esd-4-171-2013.
Goll, D. S., V. Brovkin, J. Liski, T. Raddatz, T. Thum, and K. E. O. Todd-Brown (2015), Strong dependence of CO_2 emissions from anthropogenic land cover change on soil carbon parametrization and initial land cover, *Global Biogeochem. Cycles*, *29*, 1511–1523, doi:10.1002/2014GB004988.
Hansen, M. C., et al. (2013), High-resolution global maps of 21st-century forest cover change, *Science*, *342*, 850–853, doi:10.1126/science.1244693.
Hansis, E., S. J. Davis, and J. Pongratz (2015), Relevance of methodological choices for accounting of land use change carbon fluxes, *Global Biogeochem. Cycles*, *29*, 1230–1246, doi:10.1002/2014GB004997.
He, F., Q. Ge, J. Dai, and Y. Rao (2008), Forest change of China in recent 300 years, *J. Geogr. Sci.*, *18*(1), 59–72, doi:10.1007/s11442-008-0059-8.
Houghton, R. A. (2003), Revised estimates of the annual net flux of carbon to the atmosphere from changes in land use and land management 1850–2000, *Tellus B*, *55*(2), 378–390, doi:10.1034/j.1600-0889.2003.01450.x.
Houghton, R. A. (2008), Carbon flux to the atmosphere from land-use changes: 1850–2005, in *TRENDS: A Compendium of Data on Global Change*, Carbon Dioxide Information Analysis Center, Oak Ridge National Laboratory, U.S. Department of Energy, Oak Ridge, Tenn.
Houghton, R. A., J. E. Hobbie, J. M. Melillo, B. Moore, B. J. Peterson, G. R. Shaver, and G. M. Woodwell (1983), Changes in the Carbon Content of Terrestrial Biota and Soils between 1860 and 1980: A Net Release of CO_2 to the Atmosphere, *Ecol. Monogr.*, *53*(3), 236–262.
Houghton, R. A., J. I. House, J. Pongratz, G. R. Van Der Werf, R. S. Defries, M. C. Hansen, C. Le Quéré, and N. Ramankutty (2012), Carbon emissions from land use and land-cover change, *Biogeosciences*, *9*(12), 5125–5142, doi:10.5194/bg-9-5125-2012.
Huntzinger, D. N., et al. (2013), The North American carbon program multi-scale synthesis and terrestrial model intercomparison project—Part 1: Overview and experimental design, *Geosci. Model Dev.*, *6*(6), 2121–2133, doi:10.5194/gmd-6-2121-2013.
Hurtt, G. C., S. Frolking, M. G. Fearon, B. Moore, E. Shevliakova, S. Malyshev, S. W. Pacala, and R. A. Houghton (2006), The underpinnings of land-use history: Three centuries of global gridded land-use transitions, wood-harvest activity, and resulting secondary lands, *Global Change Biol.*, *12*(7), 1208–1229, doi:10.1111/j.1365-2486.2006.01150.x.
Hurtt, G. C., et al. (2011), Harmonization of land-use scenarios for the period 1500–2100: 600 years of global gridded annual land-use transitions, wood harvest, and resulting secondary lands, *Clim. Change*, *109*(1), 117–161, doi:10.1007/s10584-011-0153-2.
Imbach, P., M. Manrow, E. Barona, A. Barretto, G. Hyman, and P. Ciais (2015), Spatial and temporal contrasts in the distribution of crops and pastures across Amazonia: A new agricultural land use data set from census data since 1950, *Global Biogeochem. Cycles*, *29*, 898–916, doi:10.1002/2014GB004999.
Ito, A., and M. Inatomi (2012), Use of a process-based model for assessing the methane budgets of global terrestrial ecosystems and evaluation of uncertainty, *Biogeosciences*, *9*(2), 759–773, doi:10.5194/bg-9-759-2012.
Jain, A. K., and X. Yang (2005), Modeling the effects of two different land cover change data sets on the carbon stocks of plants and soils in concert with CO_2 and climate change, *Global Biogeochem. Cycles*, *19*, GB2015, doi:10.1029/2004GB002349.
Jain, A. K., P. Meiyappan, Y. Song, and J. I. House (2013), CO_2 emissions from land-use change affected more by nitrogen cycle, than by the choice of land-cover data, *Global Change Biol.*, *19*(9), 2893–2906, doi:10.1111/gcb.12207.
Kato, E., T. Kinoshita, A. Ito, M. Kawamiya, and Y. Yamagata (2013), Evaluation of spatially explicit emission scenario of land-use change and biomass burning using a process-based biogeochemical model, *J. Land Use Sci.*, *8*(1), 104–122, doi:10.1080/1747423X.2011.628705.
Kim, D., J. O. Sexton, and J. R. Townshend (2015), Accelerated deforestation in the humid tropics from the 1990s to the 2000s, *Geophys. Res. Lett.*, *42*, 1–7, doi:10.1002/2014GL062777.
Klein Goldewijk, K. (2001), Estimating global land use change over the past 300 years: The HYDE Database, *Global Biogeochem. Cycles*, *15*(2), 417–433, doi:10.1029/1999GB001232.
Klein Goldewijk, K., A. Beusen, G. Van Drecht, and M. De Vos (2011), The HYDE 3.1 spatially explicit database of human-induced global land-use change over the past 12,000 years, *Global Ecol. Biogeogr.*, *20*(1), 73–86, doi:10.1111/j.1466-8238.2010.00587.x.
Krinner, G., N. Viovy, N. de Noblet-Ducoudre, J. Ogee, J. Polcher, P. Friedlingstein P. Ciais, S. Sitch, and I. C. Prentice (2005), A dynamic global vegetation model for studies of the coupled atmosphere-biosphere system, *Global Biogeochem. Cycles*, *19*, GB1015, doi:10.1029/2003GB002199.
Le Quéré, C., et al. (2015), Global carbon budget 2014, *Earth Syst. Sci. Data*, *7*(1), 47–85, doi:10.5194/essd-7-47-2015.
McGuire, A. D., et al. (2001), Carbon balance of the terrestrial biosphere in the twentieth century: Analyses of CO_2, climate and land use effects with four process-based ecosystem models, *Global Biogeochem. Cycles*, *15*(1), 183–206, doi:10.1029/2000GB001298.
Meiyappan, P., and A. K. Jain (2012), Three distinct global estimates of historical land-cover change and land-use conversions for over 200 years, *Front. Earth Sci.*, *6*(2), 122–139, doi:10.1007/s11707-012-0314-2.
Oleson, K. W., et al. (2013), Technical Description of version 4.5 of the Community Land Model (CLM).
Peng, S.-S., S. Piao, Z. Zeng, P. Ciais, L. Zhou, L. Z. Li, R. B. Myneni, Y. Yin, and H. Zeng (2014), Afforestation in China cools local land surface temperature, *Proc. Natl. Acad. Sci. U.S.A.*, *111*(8), 2915–2919, doi:10.1073/pnas.1315126111.
Piao, S., P. Ciais, P. Friedlingstein, N. De Noblet-Ducoudré, P. Cadule, N. Viovy, and T. Wang (2009), Spatiotemporal patterns of terrestrial carbon cycle during the 20th century, *Global Biogeochem. Cycles*, *23*, GB4026, doi:10.1029/2008GB003339.
Pongratz, J., C. Reick, T. Raddatz, and M. Claussen (2008), A reconstruction of global agricultural areas and land cover for the last millennium, *Global Biogeochem. Cycles*, *22*, GB3018, doi:10.1029/2007GB003153.
Pongratz, J., T. Raddatz, C. H. Reick, M. Esch, and M. Claussen (2009), Effects of anthropogenic land cover change on the carbon cycle of the last millennium, *Global Biogeochem. Cycles*, *23*, GB3018, doi:10.1029/2009GB003488.
Pongratz, J., C. H. Reick, R. A. Houghton, and J. I. House (2014), Terminology as a key uncertainty in net land use and land cover change carbon flux estimates, *Earth Syst. Dyn.*, *5*(1), 177–195, doi:10.5194/esd-5-177-2014.
Poulter, B., et al. (2015), Plant functional type classification for earth system models: Results from the European Space Agency's Land Cover Climate Change Initiative, *Geosci. Model Dev.*, *8*(7), 2315–2328, doi:10.5194/gmd-8-2315-2015.
Ramankutty, N., and J. A. Foley (1999), Estimating historical changes in global land cover: Croplands from 1700 to 1992, *Global Biogeochem. Cycles*, *13*(4), 997–1027, doi:10.1029/1999GB900046.
Reick, C. H., T. Raddatz, V. Brovkin, and V. Gayler (2013), Representation of natural and anthropogenic land cover change in MPI-ESM, *J. Adv. Model. Earth Syst.*, *5*(3), 459–482, doi:10.1002/jame.20022.

Shevliakova, E., S. W. Pacala, S. Malyshev, G. C. Hurtt, P. C. D. Milly, J. P. Caspersen, L. T. Sentman, J. P. Fisk, C. Wirth, and C. Crevoisier (2009), Carbon cycling under 300 years of land use change: Importance of the secondary vegetation sink, *Global Biogeochem. Cycles*, *23*, GB2022, doi:10.1029/2007GB003176.

Sitch, S., et al. (2003), Evaluation of ecosystem dynamics, plant geography and terrestrial carbon cycling in the LPJ dynamic global vegetation model, *Global Change Biol.*, *9*(2), 161–185, doi:10.1046/j.1365-2486.2003.00569.x.

Sitch, S., et al. (2015), Recent trends and drivers of regional sources and sinks of carbon dioxide, *Biogeosciences*, *12*(3), 653–679, doi:10.5194/bg-12-653-2015.

Smith, B., I. C. Prentice, and M. T. Sykes (2001), Representation of vegetation dynamics in the modelling of terrestrial ecosystems: Comparing two contrasting approaches within European climate space, *Global Ecol. Biogeogr.*, *10*(6), 621–637.

Stocker, B. D., and F. Joos (2015), Quantifying differences in land use emission estimates implied by definition discrepancies, *Earth Syst. Dyn.*, *6*(2), 731–744, doi:10.5194/esd-6-731-2015.

Stocker, B., F. Feissli, and K. Strassmann (2014), Past and future carbon fluxes from land use change, shifting cultivation and wood harvest, *Tellus B*, *66*, 23,188, doi:10.3402/tellusb.v66.23188.

Strassmann, K. M., F. Joos, and G. Fischer (2008), Simulating effects of land use changes on carbon fluxes: Past contributions to atmospheric CO_2 increases and future commitments due to losses of terrestrial sink capacity, *Tellus, Ser. B Chem. Phys. Meteorol.*, *60*(4), 583–603, doi:10.1111/j.1600-0889.2008.00340.x.

Wilkenskjeld, S., S. Kloster, J. Pongratz, T. Raddatz, and C. H. Reick (2014), Comparing the influence of net and gross anthropogenic land-use and land-cover changes on the carbon cycle in the MPI-ESM, *Biogeosciences*, *11*(17), 4817–4828.

Zaehle, S., and A. D. Friend (2010), Carbon and nitrogen cycle dynamics in the O-CN land surface model: 1. Model description, site-scale evaluation, and sensitivity to parameter estimates, *Global Biogeochem. Cycles*, *24*, GB1005, doi:10.1029/2009GB003521.